

# Development of low radioactivity photomultiplier tubes for the XMASS-I detector

XMASS Collaboration\*

K. Abe<sup>a,e</sup>, K. Hiraide<sup>a,e</sup>, K. Ichimura<sup>a,e</sup>, Y. Kishimoto<sup>a,e</sup>, K. Kobayashi<sup>a,e</sup>,  
M. Kobayashi<sup>a</sup>, S. Moriyama<sup>a,e</sup>, M. Nakahata<sup>a,e</sup>, T. Norita<sup>a</sup>, H. Ogawa<sup>a,e,1</sup>,  
K. Sato<sup>a</sup>, H. Sekiya<sup>a,e</sup>, O. Takachio<sup>a</sup>, A. Takeda<sup>a,e</sup>, S. Tasaka<sup>a</sup>,  
M. Yamashita<sup>a,e</sup>, B. S. Yang<sup>a,e,2</sup>, N. Y. Kim<sup>b</sup>, Y. D. Kim<sup>b</sup>, Y. Itow<sup>c,f</sup>,  
K. Kanzawa<sup>c</sup>, R. Kegasa<sup>c</sup>, K. Masuda<sup>c</sup>, H. Takiya<sup>c</sup>, K. Fushimi<sup>d,3</sup>,  
G. Kanzaki<sup>d</sup>, K. Martens<sup>e</sup>, Y. Suzuki<sup>e</sup>, B. D. Xu<sup>e</sup>, R. Fujita<sup>g</sup>, K. Hosokawa<sup>g,4</sup>,  
K. Miuchi<sup>g</sup>, N. Oka<sup>g</sup>, Y. Takeuchi<sup>g,e</sup>, Y. H. Kim<sup>h,b</sup>, K. B. Lee<sup>h</sup>, M. K. Lee<sup>h</sup>,  
Y. Fukuda<sup>i</sup>, M. Miyasaka<sup>j</sup>, K. Nishijima<sup>j</sup>, S. Nakamura<sup>k</sup>

<sup>a</sup>*Kamioka Observatory, Institute for Cosmic Ray Research, the University of Tokyo,  
Higashi-Mozumi, Kamioka, Hida, Gifu, 506-1205, Japan*

<sup>b</sup>*Center for Underground Physics, Institute for Basic Science, 70 Yuseong-daero 1689-gil,  
Yuseong-gu, Daejeon, 305-811, South Korea*

<sup>c</sup>*Institute for Space-Earth Environmental Research, Nagoya University, Nagoya, Aichi  
464-8601, Japan*

<sup>d</sup>*Institute of Socio-Arts and Sciences, The University of Tokushima, 1-1  
Minamijosanjimacho Tokushima city, Tokushima, 770-8502, Japan*

<sup>e</sup>*Kavli Institute for the Physics and Mathematics of the Universe (WPI), the University of  
Tokyo, Kashiwa, Chiba, 277-8582, Japan*

<sup>f</sup>*Kobayashi-Maskawa Institute for the Origin of Particles and the Universe, Nagoya  
University, Furo-cho, Chikusa-ku, Nagoya, Aichi, 464-8602, Japan*

<sup>g</sup>*Department of Physics, Kobe University, Kobe, Hyogo 657-8501, Japan*

<sup>h</sup>*Korea Research Institute of Standards and Science, Daejeon 305-340, South Korea*

<sup>i</sup>*Department of Physics, Miyagi University of Education, Sendai, Miyagi 980-0845, Japan*

<sup>j</sup>*Department of Physics, Tokai University, Hiratsuka, Kanagawa 259-1292, Japan*

<sup>k</sup>*Department of Physics, Faculty of Engineering, Yokohama National University,  
Yokohama, Kanagawa 240-8501, Japan*

---

## Abstract

XMASS-I is a single-phase liquid xenon detector whose purpose is direct de-

---

\**E-mail address:* xmass.publications8@km.icrr.u-tokyo.ac.jp .

<sup>1</sup>Now at Department of Physics, College of Science and Technology, Nihon University, Kanda, Chiyoda-ku, Tokyo 101-8308, Japan.

<sup>2</sup>Now at Center for Axion and Precision Physics Research, Institute for Basic Science, Daejeon 34051, South Korea.

<sup>3</sup>Now at Department of Physics, Tokushima University, 2-1 Minami Josanjimacho Tokushima city, Tokushima, 770-8506, Japan

<sup>4</sup>Now at Research Center for Neutrino Science, Tohoku University, Sendai, Miyagi 980-8578, Japan.

tection of dark matter. To achieve the low background requirements necessary in the detector, a new model of photomultiplier tubes (PMTs), R10789, with a hexagonal window was developed based on the R8778 PMT used in the XMASS prototype detector. We screened the numerous component materials for their radioactivity. During development, the largest contributions to the reduction of radioactivity came from the stem and the dynode support. The glass stem was exchanged to the Kovar alloy one and the ceramic support were changed to the quartz one. R10789 is the first model of Hamamatsu Photonics K. K. that adopted these materials for low background purposes and provided a groundbreaking step for further reductions of radioactivity in PMTs. Measurements with germanium detectors showed  $1.2\pm 0.3$  mBq/PMT of  $^{226}\text{Ra}$ , less than 0.78 mBq/PMT of  $^{228}\text{Ra}$ ,  $9.1\pm 2.2$  mBq/PMT of  $^{40}\text{K}$ , and  $2.8\pm 0.2$  mBq/PMT of  $^{60}\text{Co}$ . In this paper, the radioactive details of the developed R10789 are described together with our screening methods and the components of the PMT.

*Keywords:* PMT, radioactivity, HPGe, mass spectrometry

---

## 1. Introduction

Direct detection of dark matter is one of the major scientific challenges in modern astroparticle physics. Based on the proposal [1], a single-phase liquid xenon (LXe) detector, XMASS-I was constructed [2]. Since the dark matter signal is expected to be rare, dark matter searches require low background detectors. XMASS-I is designed for dark matter and for other many rare event searches. For a spin-independent WIMP-nucleon cross section, it is designed to search as low as  $10^{-45}$  cm<sup>2</sup> for a WIMP mass of 100 GeV/ $c^2$ . To realize this sensitivity, the background level in the fiducial volume is required to be  $10^{-4}$ /day/kg/keV for deposited energies below 100 keV.

Background originating from radioactive impurities in detector materials is one of the most serious problems in a low background experiment. It is crucial to prepare materials of sufficiently low radioactivity before detector construction.

The dominant source of radioactivity in the XMASS prototype detector [3]

was the Hamamatsu R8778 photomultiplier tubes (PMTs). Though R8778 was a model developed for the XMASS prototype detector and its radioactivity was much lower than that of standard PMTs, an order of magnitude reduction of radioactivity was necessary to meet the background required for the XMASS-I detector. Therefore we developed a new model of low radioactivity PMT, R10789, based on R8778. In order to lower the background, we screened numerous candidate materials for their radioactivity.

In this paper we describe the development target in Section 2, the screening methods in Section 3 and the components of the PMT in Section 4. The radioactivity in the final product of R10789 is presented in Section 5. The development summary is described in Section 6, along with a discussion outlining the largest component contributions to the radioactivity, this is necessary to attain further reductions in future developments. The conclusion is written in Section 7.

## 2. Target of the development

Firstly, we need to define the activity level required for XMASS-I. By using Monte Carlo simulations [4] with the detector geometry at the design stage, it is estimated that radioactivity one order of magnitude lower than the R8778 PMT is required to reduce the PMT contributions to a background less than  $2 \times 10^{-5}$ /day/kg/keV for deposited energies below 100 keV [5]. Since the target of the XMASS-I detector's background is  $1 \times 10^{-4}$ /day/kg/keV, this 20% budget for the PMTs is a reasonable requirement considering contributions from other sources of background. Following this consideration, we set this as our target for the PMT development, outlined in Table 1. The Kovar alloy used in both R8778 and R10789 contains cobalt therefore the target value of  $^{60}\text{Co}$  is the same with that of the R8778 PMT.  $^{60}\text{Co}$  is generated by ambient thermal neutrons inside the cobalt metal. When R10789 was developed no other candidate material except for Kovar was known to match the small thermal contraction coefficient of the quartz window. We note that although the R8778 values listed in Table 1 only refer to the PMT, the target values include both the PMT and a voltage

divider circuit in this development as it is assumed negligible in comparison.

Table 1: The radioactivity of R8778 measured with HPGe detectors [3] and the target values for the development of the new PMT (1/10 of R8778, except for  $^{60}\text{Co}$ ) in mBq/PMT. While the numbers for R8778 only reflect the PMT itself, the shown target numbers will be applied to the sum of the PMT and its voltage divider circuit. During the target estimation, we assumed the decay equilibrium is kept for the  $^{238}\text{U}$  chain and the  $^{232}\text{Th}$  chain.

	The $^{238}\text{U}$ chain ( $^{238}\text{U}$ , $^{226}\text{Ra}$ )	$^{232}\text{Th}$ chain ( $^{232}\text{Th}$ , $^{228}\text{Ra}$ )	$^{40}\text{K}$	$^{60}\text{Co}$
PMT(R8778)	$18\pm 2$	$6.9\pm 1.3$	$140\pm 20$	$5.5\pm 0.9$
Target (PMT+circuit)	1.8	0.69	14	5.5

### 3. Material screening methods for radioactivity in the PMT

#### 3.1. High-purity germanium (HPGe) detector measurement

To measure the radioactivity of materials with sufficient sensitivity, we mainly used three low background HPGe detectors manufactured by CANBERRA. The detectors are installed at the Kamioka observatory in the Kamioka Mine under Mt. Ikenoyama, which provides 2700 m water equivalent shielding from cosmic rays. Two of them are co-axial p-type HPGe detectors with 100% and 120% relative detection efficiency <sup>5</sup> respectively, and the other is a co-axial n-type detector with 110% relative efficiency. The sample chambers are cylindrical with a diameter of roughly 15 cm and a height of 17 cm. To suppress background caused by Rn gas, these sample chambers are continuously flushed with Rn-free air in which the  $^{222}\text{Rn}$  concentration is less than a few tens of mBq/m<sup>3</sup>. Lead (175 mm) and copper (50 mm) shields cover the whole sample regions to reduce background from the outside.

<sup>5</sup> The efficiency is given relative to the efficiency of a three inch diameter three inch thick NaI(Tl) for 1.332 MeV gamma from  $^{60}\text{Co}$  source which is positioned 25 cm away from the detector.

An example of measured gamma-ray spectrum from one of our HPGe detectors is shown in Figure 1 together with its background spectrum. The measured sample is glass beads used as electrical insulation for the feedthroughs. Many peaks from the  $^{238}\text{U}$  chain, the  $^{232}\text{Th}$  chain, and  $^{40}\text{K}$  can be clearly identified. The energy region from 40 keV to 3 MeV was examined to identify radioisotopes and to quantify their amount. Typical sensitivities of a few mBq/kg for the  $^{238}\text{U}$  and the  $^{232}\text{Th}$  chains are obtained using a sample of a few kg with one week's worth of measurements. Sensitivity for  $^{60}\text{Co}$  is 3 times better than the  $^{238}\text{U}$  chain case and for  $^{40}\text{K}$  is about 10 times worse than that of the  $^{238}\text{U}$  chain, mainly due to the branching ratio to gamma rays in its decay.

By comparison of actual data and Monte Carlo simulation for three calibration sources,  $^{57}\text{Co}$ ,  $^{137}\text{Cs}$ , and  $^{60}\text{Co}$ , we estimated the systematic error of our HPGe measurements to be +30%–10%. Since the systematic error is common for all measurements, the results in following sections are shown only with their respective statistical errors.

### *3.2. Mass spectrometry for $^{238}\text{U}$ and $^{232}\text{Th}$ measurements*

We also used two methods from mass spectrometry, inductively coupled plasma mass spectrometry (ICPMS) and glow discharge mass spectrometry (GDMS) for the  $^{238}\text{U}$  and  $^{232}\text{Th}$  measurements.

Long-lived isotope often disrupt a decay chain's equilibrium, as in the  $^{238}\text{U}$  and the  $^{232}\text{Th}$  chains. For the  $^{238}\text{U}$  chain we measured  $^{238}\text{U}$  for the top part and  $^{226}\text{Ra}$  for the middle part of the  $^{238}\text{U}$  chain independently. For the  $^{232}\text{Th}$  chain  $^{232}\text{Th}$  and  $^{228}\text{Ra}$  for the part of after  $^{232}\text{Th}$  were measured. Since the branching ratios to high energy gamma-rays, which are suitable for HPGe measurements, are small, the HPGe's sensitivities to the nuclear species before  $^{226}\text{Ra}$  for U chain and to  $^{232}\text{Th}$  are very low. From these nuclear species, only low energy gamma-rays, beta-rays, and alpha rays are emitted, and due to their short interaction length, the contribution to the detector background is limited to radioisotopes

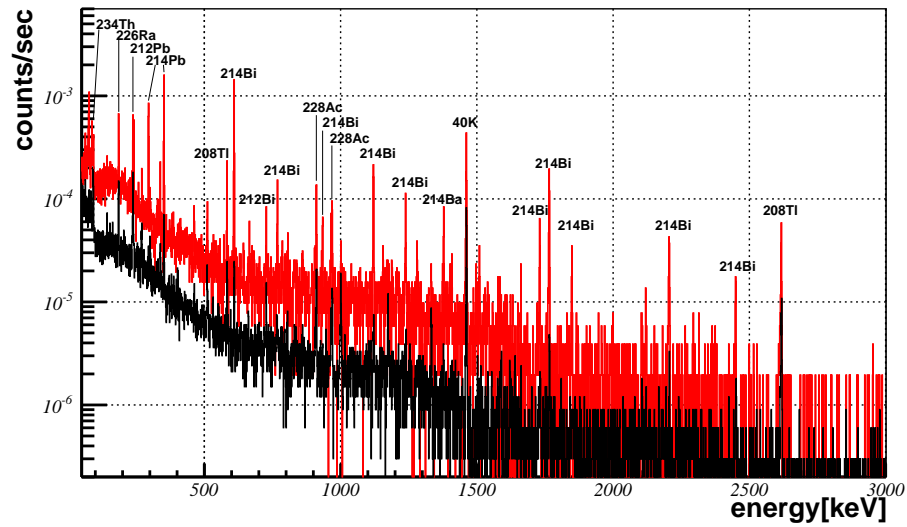


Figure 1: Typical gamma-ray spectra of a glass beads sample and a background using one of our HPGe detectors are shown. The glass beads are largely radioactive as presented in Table 3,  $1.61 \pm 0.02$  mBq/PMT for  $^{226}\text{Ra}$ ,  $0.28 \pm 0.02$  mBq/PMT for  $^{228}\text{Ra}$  and  $3.3 \pm 0.2$  mBq/PMT for  $^{40}\text{K}$ .

that are very close to the LXe inside XMASS-I <sup>6</sup> . For this reason, <sup>238</sup>U and <sup>232</sup>Th measurements by mass spectrometry were conducted only for the PMT components at the inner side of the detector, not for the voltage divider circuit.

#### 4. Components of the PMT, R10789, and the voltage divider circuit

In this section, we discuss the various component materials used in the newly developed R10789 PMT and its voltage divider circuit.

##### 4.1. The PMT(R10789)

The PMTs are divided into ten components: dynodes, electrode, two different body cylinders, stem, glass beads, lead wires, quartz, sealing, and getter. Measurements were conducted on the sample for each component.

These components are listed in Table 2, together with the weights of the measurement samples and the respective amount used to produce one PMT. The weights for the HPGc measurements were a factor 4-100 larger than what is used for one PMT. Figure 2 shows the R10789 PMT with the voltage divider circuit, and Figure 3 shows a schematic view of R10789.



Figure 2: The R10789 PMT with the voltage divider circuit.

---

<sup>6</sup> It is estimated that in XMASS-I, the background originated from neutrons as fission fragments of <sup>238</sup>U is much smaller and can be negligible compared to the one from the decay chain.

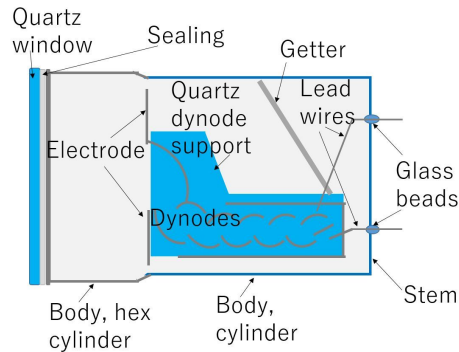


Figure 3: The schematic view of PMT R10789. The components as explained in Section 4 are shown.

There are two body components used in one R10789 PMT, both of which are made from Kovar alloy. One is a hexagonal-shape tube matching the shape of the quartz entrance window, while the rest of the body is cylindrical to which the stem is attached. The materials of the dynode support and the stem were exchanged from the ceramic and the glass in R8778 to the quartz and the Kovar alloy in R10789, respectively. The ceramic and the glass were the largest sources of radioactivity in the R8778 PMT, by reducing the amounts of the ceramic and glass in the new R10789 PMT as much as possible, a large reduction of radioactivity was achieved.

#### 4.2. The voltage divider circuit

Items in the voltage divider circuit, which include circuit parts such as resistors, capacitors and a circuit board are also presented in Table 2. Two cables, one for signal and the other for the high voltage (HV) supply, are also included in this table. Since most of the parts are small, it was possible to measure large quantities of the parts used for a few tens to hundreds of the PMTs in one measurement. This led to high precision measurements.

The cables are polytetrafluoroethylene (PTFE) insulated. The signal coaxial cable is compatible with RG196, and both the inner dielectric insulator and the outer sheath are made from PTFE. The HV cable is an AWG 22 copper



conducting wire covered with PTFE. The actual cable length in XMASS-I is about 10 m, but only the effects from 1 m near the detector surface contribute, we therefore listed the radioactivity for 1 m of the cable in Table 2.

## 5. Radioactivity for the developed R10789 PMT

The total radioactivity of the developed R10789 is summarized in this section, the unit of activity is mBq/PMT.

### 5.1. The results from measurement of each part

Tables 3 and 4 show the results of the R10789 PMT and the voltage divider circuit using the HPGe detectors. In case the center value does not exceed twice the statistical error, or is negative, we regarded the result as zero consistent and set an upper limit calculated as  $\max\{0, \text{the central value}\} + 1.28 \times \text{statistical error}$ . The total radioactivity for the PMT components and the voltage divider circuit components are shown in Table 5 along with their target values introduced above. In the calculation of the total radioactivity the central values of each component are summed up, each value's sign is included in the sum.

While the values for  $^{40}\text{K}$  and  $^{60}\text{Co}$  are significantly smaller than their targets,  $^{226}\text{Ra}$  and  $^{228}\text{Ra}$  are larger by a factor of 1.3 and 2, respectively. For  $^{226}\text{Ra}$ , the largest contribution comes from the glass beads, which accounts for about 70% of the total radioactivity  $2.3 \pm 0.3$  mBq/PMT. Other large contributions come from the coupling capacitors and the signal cable, about 10% each. These three components dominate and account for about 90% of the total. As for the  $^{228}\text{Ra}$ , the largest detected value is again from the glass beads, about 20% of the total radioactivity,  $1.6 \pm 0.3$  mBq/PMT. The getter, the coupling capacitors, the signal connectors and the signal cables also make non-negligible contribution of about 0.1 mBq/PMT <sup>7</sup>.

---

<sup>7</sup>Sum of the detected values is only a half of the total sum, the remaining half comes from many large center values in the upper limits due to their statistics error. While each value

The glass beads and the resistors are the only samples from which significant  $^{40}\text{K}$  are detected. The total  $^{60}\text{Co}$  activity is only 60% of the target. The main contribution comes from the Kovar alloy in the two PMT body parts and the stem. Another  $^{60}\text{Co}$  contribution comes from the dynodes, however it is quite small compared to the body.

---

are zero consistent within error, the sum of them exceeds twice of error.

Table 2: List of the developed R10789 parts. The weights for HPGe measurements and the weight of each component per PMT are presented together. Total weight of the parts corresponding to the one R10789 is 162.8 g.

Samples	Weight for measurement (g)	Weight per PMT (g)
<b>PMT(R10789)</b>		
Dynodes (stainless steel)	159	16.2
Electrode (stainless steel)	89.3	8.22
Body, hex cylinder (Kovar alloy)	144	34.1
Body, cylinder (Kovar alloy)	188	49.7
Stem (Kovar alloy)	289	26.7
Glass beads	164	1.81
Lead wires (Nickel)	181	1.78
Quartz (Window & dynode support)	114	23.9
Sealing (Aluminum)	10.0	0.336
Getter	1.0	0.07
<b>Voltage divider circuit and Cables</b>		
Resistors KTR10EZPF	20.4 (4300 pieces)	0.0810 (17 pieces)
Decoupling capacitors ECWU-JC9	3.56 (80 pieces)	0.178 (4 pieces)
Coupling capacitors C4520X7R3D	12.7 (200 pieces)	0.127 (2 pieces)
Circuit board (polyimide)	432	0.99
Solder Sr34 LFM48 (Sn, Ag, Cu)	25.8	0.362
Socket connectors (Brass)	16.3 (300 pieces)	1.09 (20 pieces)
Screw m2 (Stainless steel)	11.2 (100 pieces)	0.448 (4 pieces)
Terminal for HV cables (Brass)	118 (400 pieces)	0.591 (2 pieces)
Signal connectors MCX (Brass)	181 (100 pieces)	1.81 (1 piece)
PTFE fillers	2540	66.3
Signal cable	500 (50 m)	10.0 (1 m)
HV cable	670 (100 m)	6.70 (1 m)

Table 3: Results of measurements for the developed R10789 parts measured in mBq/PMT for  $^{226}\text{Ra}$ ,  $^{228}\text{Ra}$ ,  $^{228}\text{Ra}$ ,  $^{40}\text{K}$  and  $^{60}\text{Co}$  with HPGe, and for  $^{238}\text{U}$  and  $^{232}\text{Th}$  with HPGe, GDMS and ICPMS. Measuring methods for  $^{238}\text{U}$  and  $^{232}\text{Th}$  are also listed. Details of the calculation of upper limit and summation are explained in the text.

Samples	$^{226}\text{Ra}$	$^{228}\text{Ra}$	$^{40}\text{K}$	$^{60}\text{Co}$	$^{238}\text{U}$	$^{232}\text{Th}$	Method for $^{238}\text{U}$ & $^{232}\text{Th}$
<b>PMT(R10789)</b>							
Dynodes	<0.10	<0.27	<0.95	$0.11 \pm 0.04$	$<2.8 \cdot 10^{-2}$	0.15	GDMS
Electrode	<0.20	<0.17	<0.63	$<8.8 \cdot 10^{-2}$	$<1.0 \cdot 10^{-2}$	$<3.3 \cdot 10^{-3}$	GDMS
Body, hex part	<0.16	<0.35	<1.6	$1.0 \pm 0.1$	$<4.2 \cdot 10^{-2}$	$<1.4 \cdot 10^{-2}$	GDMS
Body, cylinder part	<0.18	<0.33	<1.6	$1.14 \pm 0.08$	$<6.2 \cdot 10^{-2}$	$<2.0 \cdot 10^{-2}$	GDMS
Stem	<0.14	<0.24	<1.2	$1.08 \pm 0.07$	$<3.3 \cdot 10^{-2}$	$<1.1 \cdot 10^{-3}$	GDMS
Glass beads	$1.61 \pm 0.02$	$0.28 \pm 0.02$	$3.3 \pm 0.2$	$<6.7 \cdot 10^{-3}$	$0.43 \pm 0.16$		HPGe
Lead wires	$<9.4 \cdot 10^{-3}$	$<2.3 \cdot 10^{-2}$	$<8.2 \cdot 10^{-2}$	$<4.0 \cdot 10^{-3}$	$<2.2 \cdot 10^{-3}$	$<7.2 \cdot 10^{-4}$	GDMS
Quartz	<0.18	<0.19	<2.9	$<7.5 \cdot 10^{-2}$	$<6.0 \cdot 10^{-3}$	$<1.9 \cdot 10^{-3}$	ICPMS
Sealing	$<1.2 \cdot 10^{-2}$	$(3.5 \pm 0.9) \cdot 10^{-2}$	<0.238	$<6.0 \cdot 10^{-3}$	1.3	$2.5 \cdot 10^{-2}$	ICPMS
Getter	$<6.1 \cdot 10^{-2}$	$0.10 \pm 0.04$	<0.53	$<2.2 \cdot 10^{-2}$			
<b>Sum of the PMT</b>							
(R10789) parts	$1.6 \pm 0.3$	$1.1 \pm 0.3$	<3.2	$3.4 \pm 0.2$			

Table 4: Results of HPGe measurements for the developed voltage divider circuit parts measured in mBq/PMT for  $^{226}\text{Ra}$ ,  $^{228}\text{Ra}$ ,  $^{40}\text{K}$  and  $^{60}\text{Co}$ .

Samples	$^{226}\text{Ra}$	$^{228}\text{Ra}$	$^{40}\text{K}$	$^{60}\text{Co}$
Voltage divider circuit and Cables				
Resistors KTR10E2PF	$(3.3 \pm 0.4) \cdot 10^{-2}$	$(3.5 \pm 0.4) \cdot 10^{-2}$	$0.34 \pm 0.05$	$< 2.0 \cdot 10^{-3}$
Decoupling capacitors ECWU-JC9	$< 2.4 \cdot 10^{-2}$	$< 3.0 \cdot 10^{-2}$	$< 0.41$	$< 1.2 \cdot 10^{-2}$
Coupling capacitors C4520X7R3D	$0.22 \pm 0.03$	$(8.8 \pm 1.8) \cdot 10^{-2}$	$< 0.14$	$< 6.7 \cdot 10^{-3}$
Circuit board	$(2.3 \pm 0.4) \cdot 10^{-2}$	$< 8.2 \cdot 10^{-3}$	$< 4.0 \cdot 10^{-2}$	$< 1.7 \cdot 10^{-3}$
Solder Sr34 LFM48	$< 2.6 \cdot 10^{-2}$	$< 2.0 \cdot 10^{-2}$	$< 0.44$	$< 5.8 \cdot 10^{-3}$
Socket connectors	$< 5.0 \cdot 10^{-2}$	$< 8.8 \cdot 10^{-2}$	$< 0.58$	$< 3.9 \cdot 10^{-2}$
Screw m2	$< 3.1 \cdot 10^{-2}$	$(4.9 \pm 1.4) \cdot 10^{-2}$	$< 0.19$	$< 7.5 \cdot 10^{-3}$
Terminal for HV cables	$(7.4 \pm 3.6) \cdot 10^{-3}$	$< 1.3 \cdot 10^{-2}$	$< 5.0 \cdot 10^{-2}$	$< 1.9 \cdot 10^{-3}$
Signal connectors MCX	$< 2.8 \cdot 10^{-2}$	$(8.4 \pm 2.1) \cdot 10^{-2}$	$< 0.18$	$< 1.2 \cdot 10^{-2}$
PTFE fillers	$< 0.22$	$< 0.19$	$< 1.3$	$< 3.4 \cdot 10^{-2}$
Signal cable	$0.31 \pm 0.04$	$0.15 \pm 0.03$	$< 0.37$	$< 2.0 \cdot 10^{-2}$
HV cable	$< 5.0 \cdot 10^{-2}$	$< 5.6 \cdot 10^{-2}$	$< 1.00$	$< 2.9 \cdot 10^{-2}$
Sum of the voltage divider circuit parts	$0.73 \pm 0.11$	$0.55 \pm 0.11$	$< 1.6$	$< 5.2 \cdot 10^{-2}$

Table 5: Sum of the HPGe results for the PMT(R10789) and the voltage divider circuit. The target numbers are listed also. The unit is mBq/PMT.

	$^{226}\text{Ra}$	$^{228}\text{Ra}$	$^{40}\text{K}$	$^{60}\text{Co}$
Sum of the PMT(R10789) and the circuit	$2.3\pm 0.3$	$1.6\pm 0.3$	$<3.5$	$3.3\pm 0.2$
Target (PMT+circuit)	1.8	0.69	14	5.5

### 5.2. Results for the assembled PMT

We also carried out measurements of assembled PMTs from all of the parts to check against contamination during the assembly processes. Three assembled PMTs were measured by the HPGe, and the results are shown in Table 6. A larger amount of  $^{40}\text{K}$  was detected in the assembled PMTs. This is presumably because the chemicals used for manufacturing the photo-cathode contain potassium, these chemicals were not included in the components measurements. Except for  $^{40}\text{K}$ , the summed component and assembled PMT measurements are consistent with each other, and thus we concluded that there was no significant contamination in the assembly processes.

Table 6: Results of the three assembled R10789 PMTs with the HPGe detector. The sum of the radioactivity in the PMT components in Table 2 are also presented for the reference. The unit is mBq/PMT.

Samples	$^{226}\text{Ra}$	$^{228}\text{Ra}$	$^{40}\text{K}$	$^{60}\text{Co}$
Assembled PMT (R10789)	$1.2\pm 0.3$	$<0.78$	$9.1\pm 2.2$	$2.8\pm 0.2$
Sum of the PMT parts (R10789)	$1.6\pm 0.3$	$1.1\pm 0.3$	$<3.2$	$3.4\pm 0.2$

### 5.3. Results from mass spectrometry

Table 3 shows the results for  $^{238}\text{U}$  and  $^{232}\text{Th}$ . As for  $^{238}\text{U}$ , except for the glass beads and the aluminum sealing, the measured upper limits of the top part of the  $^{238}\text{U}$  chain are much smaller and consistent with the results of  $^{226}\text{Ra}$ . The

differences between the two measurements of the glass beads and the aluminum sealing demonstrate that within these components, the decay equilibrium of the  $^{238}\text{U}$  chain is broken. The sum of  $^{238}\text{U}$  in the glass beads and the aluminum sealing is large at about 1.5 mBq/PMT, and thus the contributions from the other components can be ignored. The target for  $^{238}\text{U}$  is the same as  $^{226}\text{Ra}$ , 1.8 mBq/PMT.<sup>8</sup>

All results of  $^{232}\text{Th}$  are smaller and consistent with the results of  $^{228}\text{Ra}$ . As in the case of  $^{238}\text{U}$ , the target for  $^{232}\text{Th}$  is the same as  $^{228}\text{Ra}$ .

Since both sums of  $^{238}\text{U}$  and  $^{232}\text{Th}$  are smaller than  $^{226}\text{Ra}$  and  $^{228}\text{Ra}$ , it is enough to compare only the results of  $^{226}\text{Ra}$  and  $^{228}\text{Ra}$  to each target value, and will be discussed in the next session.

## 6. Discussion

### 6.1. Comparison to the target numbers

As a result of the development, a significant reduction of radioactivity compared to R8778 was achieved. The activities achieved for  $^{40}\text{K}$  and  $^{60}\text{Co}$  are much smaller than their target values. The  $^{40}\text{K}$  measurement of  $9.1 \pm 2.2$  mBq/PMT for the assembled PMT shown in Table 6, is larger than the sum of all its parts, however, is still smaller than its target. As already mentioned, the larger amount of  $^{40}\text{K}$  observed in the assembled PMT can be understood as a likely extra contribution coming from the photo-cathode material, which is introduced inside the PMT in the assembly process. Since it is very difficult to estimate the amount of potassium left inside of the PMT after the vapor deposition, a further investigation was not undertaken.

The final activities for  $^{226}\text{Ra}$  and  $^{228}\text{Ra}$  in the newly developed PMT and its voltage divider circuit exceed the target values, especially  $^{228}\text{Ra}$  which is a factor of two larger. Nevertheless, we should recall that the target numbers were set with a large tolerance of at least a factor of five, and therefore the activ-

---

<sup>8</sup>We assumed the secure equilibrium in our Monte Carlo simulation.

ities are allowable for the background target in XMASS-I,  $10^{-4}$ /day/kg/keV. These newly developed PMTs are used in the XMASS-I detector, by which many dark matter and rare event searches have been carried out [6–12]. The observed amount of background caused by these PMTs in the XMASS-I detector is discussed in [13].

### 6.2. Components which have largest contributions

It is valuable to summarize key improvements and significance of this development. The largest contributions to the reduction came from two items, the stem and the dynode support. In R8778, the stem was made of glass and the dynode support from ceramic. In the new PMT, R10789, Kovar alloy and quartz are used respectively. By exchanging the glass stem for one made from Kovar alloy,  $^{226}\text{Ra}$  was reduced from  $2.3\pm 0.1$  mBq/PMT to  $<0.14$  mBq/PMT, and  $^{228}\text{Ra}$  from  $2.3\pm 0.1$  mBq/PMT to  $<0.24$  mBq/PMT. By using quartz instead of ceramic for the dynode support,  $^{226}\text{Ra}$  was reduced from  $7.9\pm 0.2$  mBq/PMT to  $<6.6\cdot 10^{-2}$  mBq/PMT and  $^{228}\text{Ra}$  from  $3.1\pm 0.2$  mBq/PMT to  $<7.0\cdot 10^{-2}$  mBq/PMT. The R10789 is the first PMT of Hamamatsu Photonics K. K. adopting the Kovar alloy stem and the quartz dynode support for low background purposes. This knowledge and these materials were adopted in the development of R11410 [14–17] and R13111 [18] with improved background. This clearly indicates the development of R10789 is a groundbreaking step for further improvement of radioactivity in PMTs.

### 6.3. For further reductions

To reduce the radioactivity even further in much lower background experiments, it is necessary to deal with the high radioactive components. The glass beads include large amounts of  $^{226}\text{Ra}$ ,  $^{228}\text{Ra}$  and  $^{40}\text{K}$ ,  $^{226}\text{Ra}$  accounts for 70% of the total. Some parts of the voltage divider circuit, such as the coupling capacitors, and the signal cable also have a large amount of  $^{226}\text{Ra}$  and  $^{228}\text{Ra}$ . In the capacitors and the signal cables, ceramic and PTFE are used respectively



as raw materials. These two materials and glass mentioned above generally contain non-negligible amounts of radioactive impurities. Therefore, to use these materials, it is quite essential to find materials with lesser radio impurities and to reduce their usage as much as possible.

As for  $^{40}\text{K}$ , a larger amount was found in the assembled PMTs than was expected from the sum of its parts, this is speculated to come from the photocathode. Chemicals used while treating the photocathode contain potassium, and therefore it is not easy to suppress this  $^{40}\text{K}$  contamination but to control it would be essential for next generation ultra-low-background PMTs. To reduce  $^{60}\text{Co}$ , Kovar alloy parts (body cylinders and stem) must be replaced with a new material whose thermal contraction coefficient matches that of quartz and does not contain cobalt. The Co-free alloy which is used for example by the R11410 PMT [17] could be used.

In our screening, there were many items where only upper limits were set. These could contribute significantly in future PMT developments, especially  $^{228}\text{Ra}$  and  $^{40}\text{K}$ . Higher sensitivity measurements are strongly demanded for further reductions.

## 7. Conclusion

We succeeded in developing the new low background PMT, R10789, which satisfies the requirements of the XMASS-I detector. It achieved large reduction factor of 8, 4, 1.7 and more than 10 from PMT R8778 for  $^{226}\text{Ra}$ ,  $^{228}\text{Ra}$ ,  $^{60}\text{Co}$ , and  $^{40}\text{K}$ , respectively. These facts prove that it can be utilized in various low background experiments. The largest contributions to the reduction were obtained by exchanging two items, the stem glass with Kovar alloy and the ceramic dynode support with quartz. This is the first model of Hamamatsu Photonics K. K. PMTs that adopted these materials for low background purposes and provided a groundbreaking step for further improvements of radioactivity in PMTs.

## Acknowledgments

We thank Hamamatsu Photonics K. K. for the cooperation in producing the low RI PMTs. We gratefully acknowledge the cooperation of Kamioka Mining and Smelting Company. This work was supported by the Japanese Ministry of Education, Culture, Sports, Science and Technology, Grant-in-Aid for Scientific Research, ICRR Joint-Usage, JSPS KAKENHI Grant Number, 19GS0204 and 26104004, and partially by the National Research Foundation of Korea Grant (NRF-2011-220-C00006) and Institute for Basic Science (IBS-R017-G1-2018-a00).

## References

### References

- [1] Y. Suzuki, arXiv:hep-ph/0008296.
- [2] K. Abe *et al.*, Nucl. Instrum. Meth. A 716 (2013) 78.
- [3] A. Minamino *et al.*, Astropart. Phys. 35 (2012) 609.
- [4] S. Agostinelli *et al.*, Nucl. Instrum. Meth. A 506 (2003) 250. ; J. Allison *et al.*, IEEE Trans. Nucl. Sci. 53 No. 1 (2006) 270.
- [5] K. Abe *et al.*, J. Phys.: Conf. Ser. 120 (2008) 042022
- [6] K. Abe *et al.*, Prog. Theor. Exp. Phys. 2018 (2018) 053D03
- [7] K. Abe *et al.*, Physical Review D 97, 102006 (2018)
- [8] K. Abe *et al.*, Prog. Theor. Exp. Phys. 2017, 103C01
- [9] K. Abe *et al.*, Physical Review Letters, 113, 121301 (2014)
- [10] K. Abe *et al.*, Prog. Theor. Exp. Phys. 2014, 063C01
- [11] K. Abe *et al.*, Phys. Lett. B 724 (2013) 46
- [12] K. Abe *et al.*, Phys. Lett. B 719 (2013) 78

- [13] K. Abe *et al.*, Phys. Lett. B 789 (2019) 45.
- [14] E. Aprile *et al.*, Astropart. Phys. 35 (2011) 43.
- [15] D. S. Akerib *et al.*, Nucl. Instrum. Meth. A 703 (2013) 1.
- [16] X. Cao *et al.*, Sci. China. Phys. Mech. Astron. 57 (2014) 1476.
- [17] E. Aprile *et al.*, Eur. Phys. J. C 75 (2015) no.11, 546.
- [18] K. Abe *et al.*, PoS ICHEP2016(2017) 1175.